Twenty-Seventh Symposium (International) on Combustion/The Combustion Institute, 1998/pp. 2757–2766

A UNIFIED ANALYSIS FOR FIRE PLUMES

J. G. QUINTIERE AND B. S. GROVE
Department of Fire Protection Engineering
0151 Engineering Building
University of Maryland
College Park, MD 20742-3031, USA

A unified analysis based on an integral approach is presented for fire plumes involving finite axisymmetric and rectangular sources. The analysis, using Gaussian profiles, obtains the best fits to experimental data found in the literature. Phenomenological constants in the theory are found to give consistent results in that coefficients expected to be numerically similar by theory are found similar among the various data sets. Thorough reviews of the literature data for line and rectangular sources are presented and yield consensus correlations, accordingly. The effect of flame radiation is explicitly included by a radiation fraction that proves to be a significant variable, previously overlooked in experiments. Effective entrainment coefficients for the far-field noncombusting plume are found to be 0.09 to 0.10, and for the flame region about 0.22 for the axisymmetric and rectangle cases as long as $D/L > 0.1$. For $D/L < 0.1$, the infinite line gives nearly double the flame entrainment. Generalized results are presented for entrainment rate and flame height in terms of single algebraic equations that span a wide range of Q^* or energy release rate values. For low Q^* fires, the effect of diameter and line width are important and expressed by the theory but not enough to address dependence involving Grashof and possibly Froude number effects near the origin. Laminar results are also addressed.

Introduction

Many have studied fire plumes, with most attention on axisymmetric rather than line or other geometric plume sources [1–15]. Theoretical analyses are principally couched in terms of assumed similarity velocity and temperature distributions, with Gaussian profiles proving adequate for the noncombusting region (e.g., Rouse et al. [2]). Turbulent mixing is taken into account by an entrainment rule based on the axial plume velocity or its momentum to account for density effects. Often, idealized point source solutions (e.g., [3,8]) for noncombusting plumes are used to describe the results for combusting plumes using an origin offset, virtual source, to adjust the data (e.g., [7]). Steward [10,11] developed integral solutions to both finite line and axisymmetric fire plumes that lead to rather complex algebraic results, which might have discouraged their use. Thomas et al. [16] show that the flame geometry has a significant influence on the power law behavior for flame height. Delichatsios [17] used these flame geometry characteristics to derive entrainment and flame height results for axisymmetric fires that are consistent with data, thereby showing the intimacy of entrainment and flame height. One of the earliest and most comprehensive studies of plumes from small fire sources was done by Yokoi [1]. He was first to point out that the axial velocity, w_{in}, the axial temperature rise, $T - T_o$, and position, z, are related by the constancy of $w_{in}^2/[(T - T_o)/T_o g z]$. We will show that this constant differs slightly in the flame and noncombusting regions.

This study will demonstrate how a theory can unify experimental correlations for fire plumes—dissecting them into two regions: the "near-field" combustion zone and the "far field," having a point source character. An integral analysis will be used for each plume geometry and a second-order correction will be applied in the near-field solution to determine better results for flame height and flame entrainment. All numerical coefficients of the theoretical results will be determined from the available ensemble of data. We shall address finite axisymmetric, line, and rectangular fire sources of width D and (longer) length L. Turbulent analyses will be considered, but we will draw on the laminar results of Roper et al. [18,19] to fully describe the data in the literature.

This work was motivated by the need to synthesize the literature results for line plumes. Yuan and Cox [14] recently reviewed the line plume literature and also presented some new data. Whereas they examined the numerous correlations, we examined the available data in the literature to establish overall correlations with our theory. In many cases, we have only plotted representative data in the summarizing figures to follow.

Model Formulation

A point (or infinite line) source model is used for both the near- and far-field domains. Hence, the base dimensions, D and D/L, become zero. We make the following additional assumptions:

1. We use the Bousinnesq assumption in which density constant, except in the buoyancy term and all other fluid properties are constant. A more complete solution might involve a correction factor in terms of T_f/T_o, which would only be absorbed into our correlation constants.
2. Gaussian profiles are used for w/w_m and $(T - T_o)/(T_m - T_o)$ in both regions for consistency, although we have no justification for using it in the near field. For example,

$$\frac{T - T_o}{T_m - T_o} = \exp\left[-\beta\left(\frac{r}{b}\right)^2\right] \qquad (1)$$

where β is selected as 1 for the near field and the rectangular source analysis.
3. Entrainment is based on a constant entrainment, α, which is the ratio of the entrainment to axial velocity. Alternatively, representing the entrainment coefficient as a momentum ratio, which would introduce $(\rho/\rho_o)^{1/2}$, another property effect, ignored here.
4. The energy release rate is assumed to be uniformly distributed in the combustion zone and directly determined from the entrainment rate by the quantity, $\Delta H_c/sn$, where ΔH_c is the heat of combustion, s is the stoichiometric air-to-fuel ratio, and n is the ratio of air entrained to air involved in combustion. The last term, n, is solely a fluid dynamic factor characteristic of the mixing in the plume. $\Delta H_c/s$ was taken as 2.91 kJ/g, corresponding to methane, for our computations.
5. Flame radiation is accounted for by a constant fraction, X_r.
6. Mass, momentum, and energy flow rates of the supplied fuel are small and ignored for these buoyancy-dominated plumes.
7. The plume is fully turbulent.

Combusting Plume Structure: Axial Temperature and Velocity

The details of the integral solutions are common in the literature (e.g., [3,8,10]), and the specifics for our results are found in the thesis by Grove [20]. Dimensionless variables are introduced as follows:

$$\Phi = \frac{T - T_o}{T_o}, \qquad W = \frac{w_m}{(gZ_c)^{1/2}}$$

$$B = \frac{b}{Z_c} \quad \text{and} \quad \zeta = \frac{z}{Z_c} \qquad (2)$$

where the characteristic plume dimension, Z_c, is given as

$$Z^* = \left(\frac{Q}{\rho_o c_p T_o g^{1/2}}\right)^{2/5}, \quad Q_D^* = \left(\frac{Z^*}{D}\right)^{5/2}$$

$$\text{and } Z^{**} = \left(\frac{Q'}{\rho_o c_p T_o g^{1/2}}\right)^{2/3}, \quad Q_D^{**} = \left(\frac{Z^{**}}{D}\right)^{3/2} \qquad (3)$$

for the axisymmetric and line plumes, respectively. The solutions can be expressed in power relationships as

$$B = C_1\zeta^m, \quad W = C_v\zeta^n \quad \text{and} \quad \Phi = C_T\zeta^p \qquad (4)$$

The theoretical solutions and the experimentally determined coefficients are given in Tables 1 and 2. We used the alcohol data of Yokoi [1] to determine the coefficients for the axisymmetric far field, using a representative fuel value of $X_r = 0.2$. The temperature and velocity data for the infinite line source are shown in Figs. 1 and 2 for the array of data found in the literature [1,2,8,12,14,15,22]. Here we assigned a value of $X_r = 0.3$ [29], representative of propane data [12], and derive the empirical coefficients accordingly. We find $C_T = 2.6$, the same as Yuan and Cox [14]. In the combusting zone, the parameter

$$\Psi = \frac{(1 - X_r)(\Delta H_c/s)}{c_p T_o} \qquad (5)$$

occurs in the solution. Except for variations in X_r, Ψ is nearly a constant for all of these data. The empirical coefficients (C's) shown in Table 2 are nearly identical for velocity and differ somewhat for temperature. The C_T value here depends on the accuracy of the flame temperature measurement. For the axisymmetric case, we have used the results of McCaffrey, who reported ΔT of about 800 °C [4], to obtain $C_T = 0.347\Psi$. However, Cox and Chitty [23] found the flame temperature for natural gas in square burners to be 960 to 980 °C for corrected thermocouple measurements, which would increase C_T to 0.427Ψ. For large pool fires where smoke blockage causes X_r to become zero, the maximum temperature rise is indicated to be roughly 1000 to 1250 °C, corresponding to the uncertainty in our coefficients: $C_T = 0.347\Psi$ to 0.427Ψ. These temperatures are consistent with data presented by Baum and McCaffrey [24] for D ranging from 6 to 30 m.

In Tables 1 and 2, we note the constancy of the parameter, $W^2/\Phi\zeta$, being approximately 1.6 and 1.4 in the far and near fields, respectively, for both geometries. The α values only vary from approximately 0.09 to 0.1 in the far fields but differ significantly for the near fields. The far field values of α and β are very sensitive to the selection of the fitted coefficients, C_V and C_T. Also, our values of α are lower than those found without explicit inclusion of X_r. For example, we find for the axisymmetric far field, α =

TABLE 1
Far-field correlations: Coefficients = theory, experiment

Dimensionless Variable	Axisymmetric (χ_r = 0.20 for data)	Infinite Line (χ_r = 0.30 for data)
B	$C_1\zeta$ $C_1 = \frac{6}{5}\alpha$, 0.118	$C_1\zeta$ $C_1 = \frac{2}{\sqrt{\pi}}\alpha$, 0.103
W	$C_v\zeta^{-1/3}$ $C_v = \left[\left(\frac{25}{24\pi}\right)\left(\frac{\beta+1}{\beta}\right)\alpha^{-2}(1-\chi_r)\right]^{1/3}$ $C_v = 4.17(1-\chi_r)^{1/3}$	$C_v\zeta^0$ $C_v = \left[\left(\frac{\beta+1}{2\beta}\right)^{1/6}\alpha^{-1/3}(1-\chi_r)^{1/3}\right.$ $C_v = 2.25(1-\chi_r)^{1/3}$
Φ	$C_T\zeta^{-5/3}$ $C_T = \left[\frac{2}{3}\left(\frac{25}{24\pi}\right)^{2/3}\frac{(\beta+1)^{2/3}}{\beta^{-1/3}\alpha^{4/3}}(1-\chi_r)^{2/3}\right]$ $C_T = 10.58(1-\chi_r)^{2/3}$	$C_T\zeta^{-1}$ $C_T = \left[\frac{(\beta+1)^{1/3}}{2^{5/6}\beta^{-1/6}}\alpha^{-2/3}(1-\chi_r)^{2/3}\right]$ $C_T = 3.30(1-\chi_r)^{2/3}$
$\frac{W^2}{\Phi\zeta}$	$\frac{3}{2}\beta$, 1.64	$\sqrt{\frac{2}{\beta}}$, 1.54
α	0.098	0.091
β	0.913	0.845

0.098 whereas Zukoski [21] reports 0.11. In the flame region, α values were derived from the respective flame height analyses, which will be discussed in the following.

Entrainment

The entrainment rates from the integral solutions follow from:

$$\frac{d\dot{m}_e}{dz} = 2\pi\rho_o \frac{d}{dz}\int_0^\infty rwdr$$

$$\text{or } \dot{m}_e = \pi\rho_o w_m b^2 \qquad (6a)$$

and

$$\frac{d\dot{m}'_e}{dz} = 2\rho_{o_0} \frac{d}{dz}\int_0^\infty wdy$$

$$\text{or } \dot{m}'_e = \pi^{1/2}\rho_o w_m b \qquad (6b)$$

The far field results follow in Table 3 using the coefficients listed in Table 1. For the axisymmetric case we C_e = 0.17, while Zukoski [21] finds 0.21 and Ricou and Spalding [30] give 0.18. For the line case, we obtain 0.36 from Table 1, whereas Yuan and Cox [14] find 0.51 from experiment. Our value is low due to our choice of C_V, which is clearly subject to error from the scatter in Fig. 2.

In the near field, we seek to find a solution that now accounts for the finite fuel source. Thomas [9] was first to argue that flame perimeter is key to determining entrainment into the flame, and Zukoski [25] needed this argument to explain his entrainment data within the continuous flame zone for burners of D = 0.19 and 0.50 m. We account for this fuel geometry effect by expressing the next-order solution to be as

$$B = \frac{D}{2Z_c} + C_1\zeta \qquad (7)$$

Substituting equation 7 into equation 6, along with w_m and C_1 from Table 2, gives the entrainment results in Table 4 for the near-field flame region. The form of the result is

$$\frac{\dot{m}_e}{\rho_o g^{1/2} D^{5/2}} = C_e\left(\frac{z}{D}\right)^{1/2}\left[1 + 2C_1\left(\frac{z}{D}\right)\right]^2 \qquad (8)$$

for the axisymmetric case and similarly for the line case as show in Table 4.

The best fit for C_1 comes from the flame height data and leads to the α values listed in Table 2. These entrainment coefficients are just modeling constants used to account for mixing; however, they may be inadequate to address pressure contributions to entrainment near the base of the plume as described by Smith et al. [26]. We speculate that the distinctly larger value of α for the line fire region is due to the enhanced mixing from distinct "fire whirl" structures that tend to occur near its base.

The C_e for the axisymmetric case comes from the best fit of the Zukoski data [25] shown in Fig. 3. This is the first unified single-equation correlation of such entrainment data. No flame entrainment data exist for the line plume, so we are stymied on a direct

TABLE 2
Near-field correlations: Coefficients = theory, experiment

Dimensionless Variable	Axisymmetric (χ_r = 0.20 for data)	Infinite Line (χ_r = 0.30 for data)
B	$C_l\zeta$ $C_l = \frac{4}{5}\alpha$, 0.179	$C_l\zeta$ $C_l = \frac{4\alpha}{3\sqrt{\pi}}$, 0.444
W	$C_v\zeta^{1/2}$ $C_v = \sqrt{\frac{4}{3}\frac{\Psi}{n}}$, 2.02 or $0.720\sqrt{\Psi}$	$C_v\zeta^{1/2}$ $C_v = \sqrt{\frac{\Psi}{n}}$, 2.3 or $0.877\sqrt{\Psi}$
Φ	$C_T\zeta^0$ $C_T = 2\frac{\Psi}{n}$, 2.73 or 0.347Ψ	$C_T\zeta^0$ $C_T = \sqrt{2}\frac{\Psi}{n}$, 3.1 or 0.450Ψ
$\frac{W^2}{\Phi\zeta}$	$\frac{3}{2}\beta$, 1.50	$\sqrt{\frac{2}{\beta}}$, 1.41
α	0.22	0.590
β	1	1

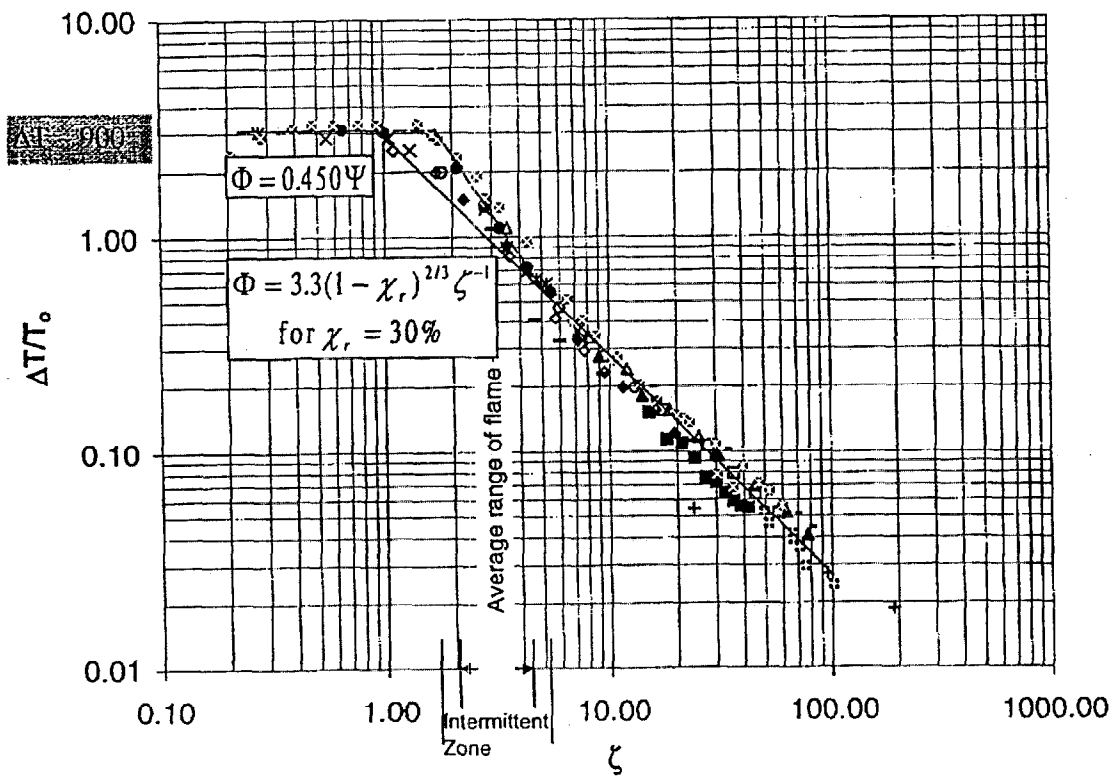

FIG. 1. Dimensionless temperature versus height for the infinite line, X_r = 30%. ■ Yokoi, 6.86 kW/m [1]; ▲ Hasemi and Nishita, 6.4 kW/m [12]; ♦ Hasemi, 52 kW/m; ● Hasemi, 342 kW/m; □ Hasemi, 13.7 kW/m; △ Hasemi, 25.2 kW/m; ○ Hasemi, 67 kW/m; ◇ Hasemi, 146 kW/m; × Hasemi, 215 kW/m; ✳ Hasemi, 296 kW/m; — Sugawa et al., 6.86 kW/m [13]; + Brodowicz and Kierkus, 9.75 × 10^{-3}) kW/m [22]; – Lee and Emmons, (Acetone), 7.087 kW/m [8]; ❄ Lee (Acetone), 11.4 kW/m; ❖ Rouse et al., 0.753–1.17 kW/m [2]; ❄ Yuan & Cox, 2–110 kW [14].

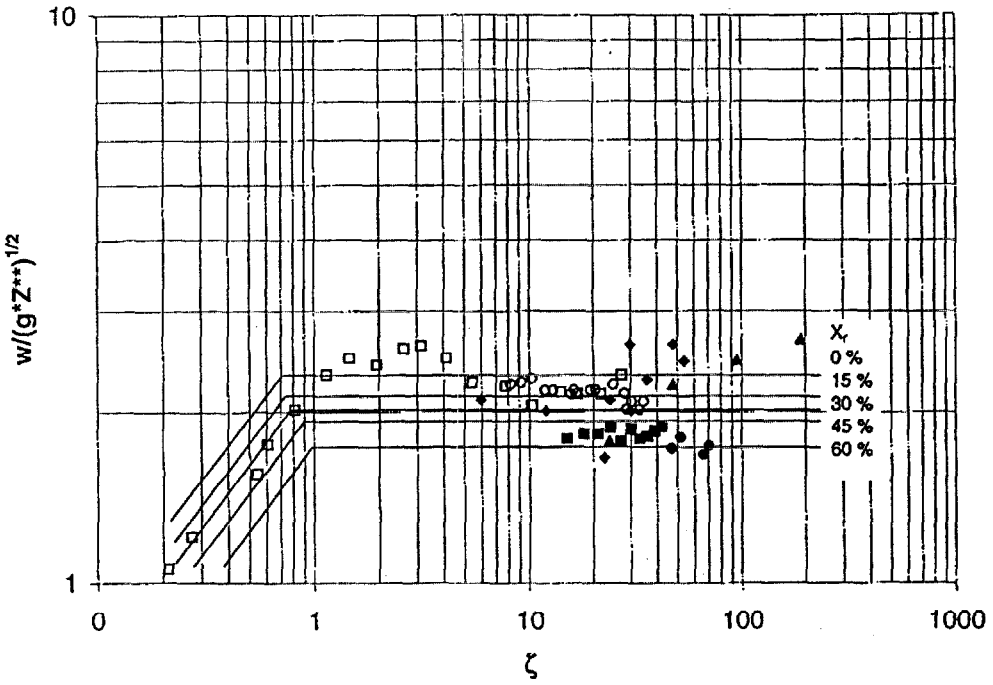

FIG. 2. Velocity radiation curves for the infinite line, initial X_r = 30%. ♦ Sugawa et al., D = 1 cm [15]; ■ Yokoi, D = 1 cm [1]; ▲ Brodowicz and Kierkus, D = .075 mm [22]; ● Rouse, Yih, & Humphreys [2]; □ Yuan & Cox, D = 1.5 cm [14]; ○ Yuan & Cox, D = 5 cm.

TABLE 3
Far-field Entrainment correlations: Coefficients = theory, experiment

Axisymmetric (χ_r = 0.20 for data)

$$\frac{\dot{m}_e}{\rho_o\sqrt{gzz^2}} = C_e\zeta^{-5/6}$$

$C_3 = \pi C_v C_f^2$, 0.17

Infinite Line (χ_r = 0.30 for data)

$$\frac{\dot{m}'_e}{\rho_o\sqrt{gzz}} = C_e\zeta^{-1/2}$$

$C_e = \sqrt{\pi}C_vC_l$, 0.364

TABLE 4
Near-field entrainment correlations: Coefficients = theory, experiment

Axisymmetric (χ_r = 0.30 for data)

$$\frac{\dot{m}_e}{\rho_o\sqrt{gDD^2}} = C_e\left(\frac{z}{D}\right)^{1/2}\left(1 + 2C_l\left(\frac{z}{D}\right)\right)^2$$

$C_e = \frac{\pi}{2\sqrt{3}}\sqrt{\frac{\Psi}{n}}$, 0.148 or $0.0565\sqrt{\Psi}$

$C_l = \frac{4}{5}\alpha$, 0.179

Infinite Line (χ_r = 0.30 for data)

$$\frac{\dot{m}'_e}{\rho_o\sqrt{gDD}} = C_e\left(\frac{z}{D}\right)^{1/2}\left(1 + 2C_l\left(\frac{z}{D}\right)\right)$$

$C_e = \frac{\sqrt{\pi}}{2}\sqrt{\frac{\Psi}{n}}$, 0.148 or $0.0565\sqrt{\Psi}$

$C_l = \frac{4\alpha}{3\sqrt{\pi}}$, 0.444

data fit for this C_e. However, we note from the theory that these coefficients are nearly equal (and not dependent on entrainment), that is, $\pi/(2\sqrt{3}) \approx \pi^{1/2}/2$. Therefore, we select the same C_e for the infinite line as in the axisymmetric case, $C_e = 0.0565\Psi^{1/2}$.

Flame Height

The deduction of flame height comes from Assumption 4, giving

$$Q = \dot{m}_e(Z_f)\frac{\Delta H_c}{ns}$$

$$\text{or } Q^*_D = \left(\frac{\dot{m}_e}{\rho_o g^{1/2}D^{5/2}}\right)\frac{\Psi}{n(1 - X_r)} \quad (9)$$

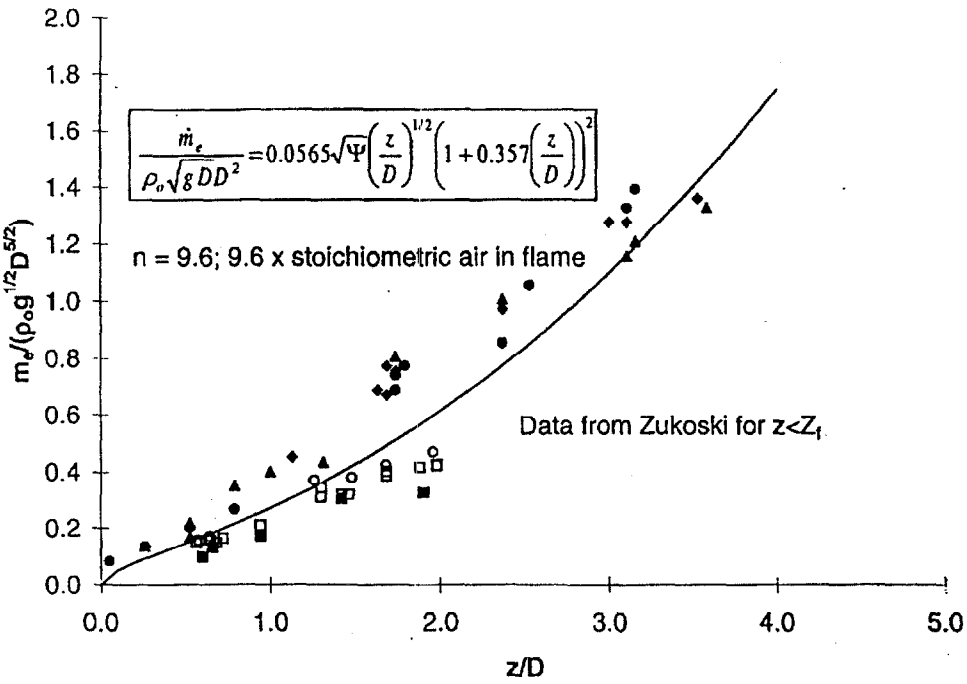

FIG. 3. Near-field axisymmetric dimensionless entrainment versus height, X_r = 30%. • Q = 21 kW (D = .19 m) [21]; ♦ Q = 42 kW (D = .19 m); ▲ Q = 63 kW (D = .19 m); ■ Q = 21 kW (D = .50 m); ○ Q = 42 kW (D = .50 m).

TABLE 5
Flame height correlations: Coefficients = theory, experiment

Axisymmetric (χ_r = 0.30 for data)

$$Q_D^* = \left(\frac{Z^*}{D}\right)^{5/2} = C_f\left(\frac{Z_f}{D}\right)^{1/2}\left(1 + 2C_l\left(\frac{Z_f}{D}\right)\right)^2$$

$$C_f = \frac{\pi}{2\sqrt{3}}\frac{(\Phi/n)^{3/2}}{(1-\chi_r)},\ 0.152 \text{ or } 0.00590\frac{\Psi^{3/2}}{(1-\chi_r)}$$

$$C_l = \frac{4}{5}\alpha,\ 0.179$$

Infinite Line (χ_r = 0.30 for data)

$$Q_D^{**} = \left(\frac{Z^{**}}{D}\right)^{3/2} = C_f\left(\frac{Z_f}{D}\right)^{1/2}\left(1 + 2C_l\left(\frac{Z_f}{D}\right)\right)$$

$$C_f = \frac{\sqrt{\pi}}{2}\frac{(\Psi/n)^{3/2}}{(1-\chi_r)},\ 0.152 \text{ or } 0.00590\frac{\Psi^{3/2}}{(1-\chi_r)}$$

$$C_l = \frac{4\alpha}{3\sqrt{\pi}},\ 0.444$$

and similarly for the line case. By making this connection between equation 9 and Table 4, we easily obtain Table 5. The lead coefficient, C_f, for the axisymmetric case was determined from the data shown in Fig. 4 as presented by Zukoski [6]. The Heskestad [7] correlation is also shown for comparison. We selected the same value of C_f for the line flames based on their approximate equality as given by theory. The C_l values for each of the geometries were found by the best fits to their respective flame height data and are given in Tables 4 and 5, accordingly. The fit to the line flame height data is shown in Fig. 5 where we plot all of the (representative) data [8–15]. We have favored the data by Yuan and Cox [14] and Hasemi and Nishita [12], and we do not have an explanation for the parallel set of data.

A value of n can be deduced, independent of the theoretical profile effects, from equation 9, which gives $C_f = C_e\,[\Delta H_c/(nsc_pT_o)]$. Using the empirical coefficients from Tables 4 and 5, we obtain n = 9.6 for both plumes, consistent with results by Taminini [28].

Some of the difficulties for the correlations to match all of the data may be due to laminar flow effects. Yuan and Cox [14] have assigned their data below Z^{**}/D = 7 as laminar. We suspect that both Grashof ($Gr = gD^3/\upsilon^2$) and Froude ($Fr = \omega(0)/(gD)^{1/2}$) numbers are important factors for both laminar and turbulent domains. From the work of Roper et al. [18,19], we can express solutions to laminar flames as

Axisymmetric:

$$\frac{Z_f}{D} \sim \left(\frac{1-X_r}{\Psi}\right) Q_D^*\, Gr^{1/2}, \text{ and}$$

Line or slot (buoyancy controlled):

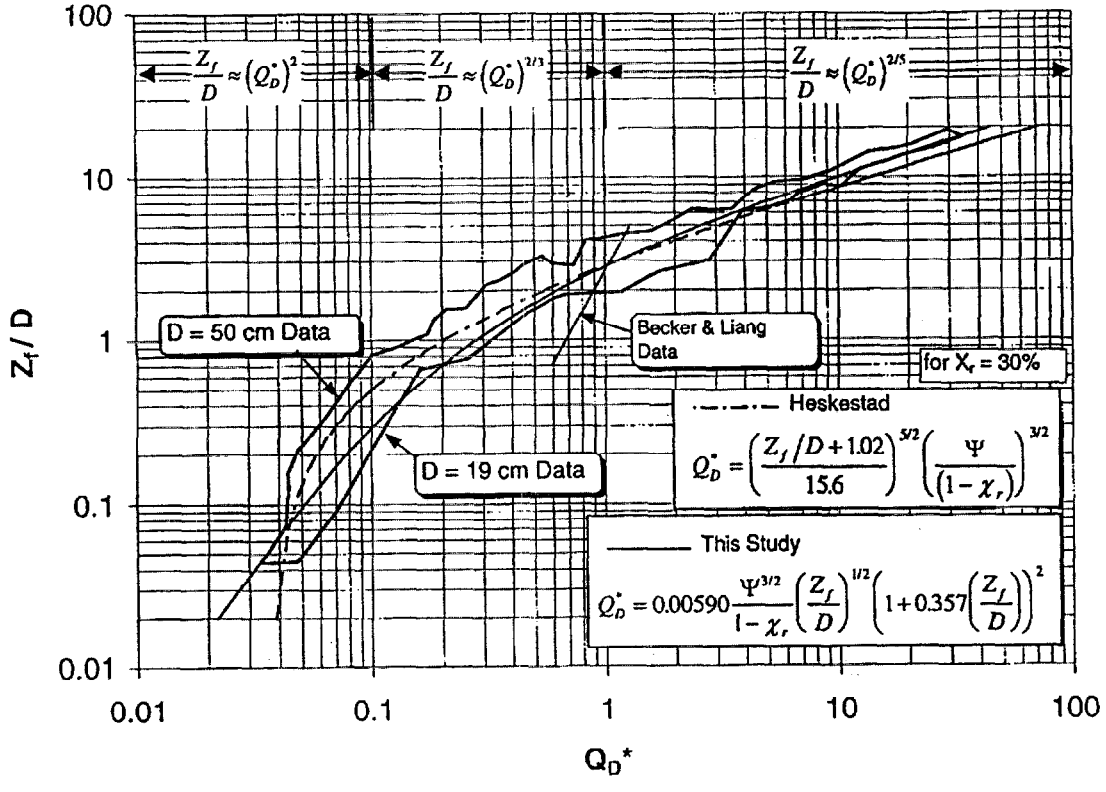

FIG. 4. Axisymmetric smooth fit of dimensionless flame height, Z_f/D, versus energy release rate, Q_D^*.

$$\frac{Z_f}{D} \sim \left[\left(\frac{1 - X_r}{\Psi}\right) Q_D^{**}\, Gr^{1/4}\right]^{4/3} \tag{10}$$

The 4/3 power result for the line case does fit the laminar data given by Yuan and Cox [14]. The data listed by McCaffrey [27] of Becker and Liang (Fig. 4), suggesting possible laminar effects, are instead for very large diameter fires and follow a two-power behavior. More significantly, the low Q_D^* region needs more attention because natural fires tend to fall between Q_D^* values of 0.05 and 5 [27].

Rectangular Fire Sources

Yokoi [1] and recently Hasemi and Nishihata [12] investigated rectangular burner fire plumes, with the latter study addressing larger propane fires (D = 0.1–1.0 m up to 150 kW). Our analysis is extended to these finite sources by the following specifications:

1. Gaussian profiles, $\beta = 1$, that is, $\exp\{-[(x/a)^2 + (y/b)^2]\}$.
2. $W^2/\Phi\zeta = C^2$, a constant, which we found to be nearly identical for the line and axisymmetric cases with a C of about 1.5, varying for the far and near fields.
3. Geometrical effects are addressed by representing: $a = L/2 + C_1 z$, and $b = D/2 + C_1 z$ as done in equation 7, but we apply this now for both the near- and far-field regions.

In the far field, the energy equation yields

$$Q(1 - X_r) = 4 \int_0^\infty \int_0^\infty \rho_0 c_p w(T - T_0)\, dx\, dy \tag{11}$$

By applying the conditions 1–3, we can solve for the temperature:

$$Q_{\text{inod}}^*(1 - X_r) = \frac{\pi}{8} C\, \Phi^{3/2} \left(\frac{z}{D}\right)^{1/2} \times \left[1 + 2C_1 \left(\frac{z}{D}\right)\right]\left[1 + 2C_1 \left(\frac{D}{L}\right)\left(\frac{z}{D}\right)\right]$$

$$Q_{\text{inod}}^* = \frac{\dot{Q}}{\rho_0 c_p T_0 g^{1/2} D^{3/2} L} \tag{12}$$

Explicitly,

$$\Phi = C_T \zeta_{\text{inod}}^{-1},\ \zeta_{\text{inod}} = \left[\frac{\left(\frac{z}{D}\right)^{1/2}\left[1 + 2C_1\left(\frac{z}{D}\right)\right]\left[1 + 2C_1\left(\frac{D}{L}\right)\left(\frac{z}{D}\right)\right]}{Q_{\text{inod}}^*}\right]^{2/3} \tag{13}$$

We have chosen $C_1 = (6/5)\alpha = 0.132$, which corresponds to the axisymmetric far-field α of 0.11 for

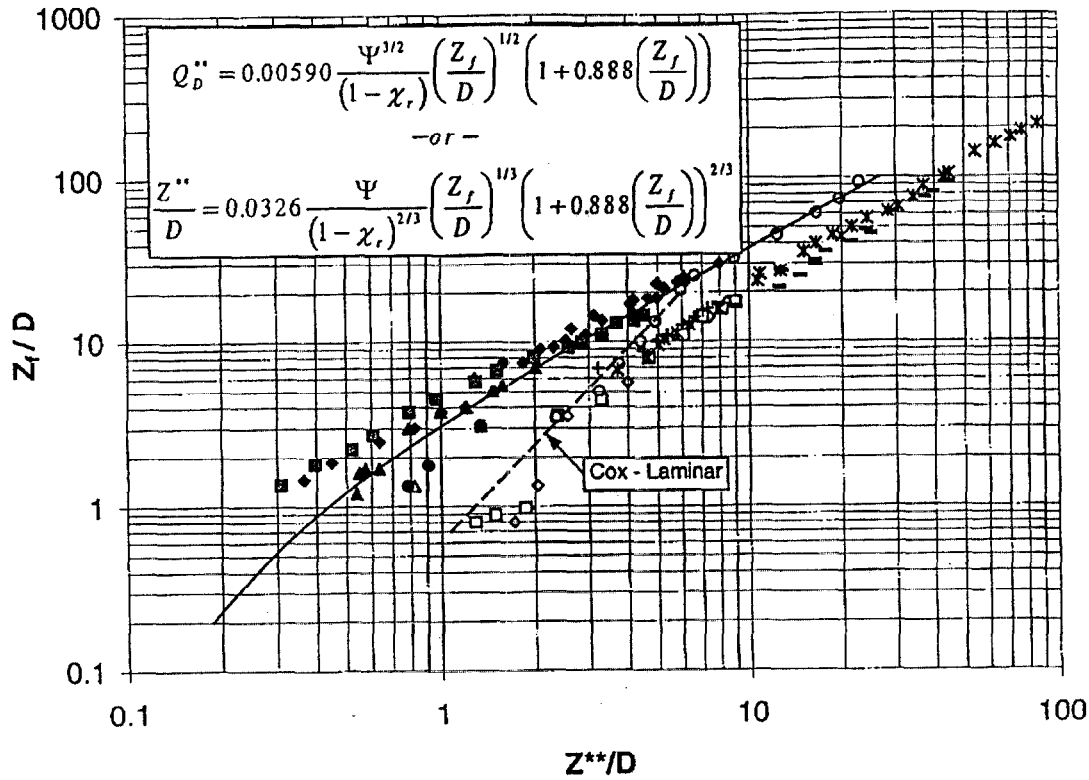

FIG. 5. Dimensionless flame height equation for the infinite line. ♦ Sugawa et al. [15]; ■ Hasemi and Nishita (D = 10 cm) [12]; ▲ Thomas [9]; ● Lee and Emmons (Asb/Methanol) (D = 1.43 cm) [8]; ◇ Lee(Asb/Acetone) (D = 1.43 cm); □ Lee(Al/Acetone) (D = 1.43 cm); △ Lee (Al/Methanol) (D = 1.43 cm); ○ Yuan & Cox (D = 1.5 cm) [14]; ✳ Steward (Propane) [10]; + Steward (Methane); ▬ Steward (Hydrogen).

$\beta = 1$ given by Zukoski [21]. Our fit to the data of Hasemi et al. [12] is shown in Fig. 6. We find C_T = 2.3 or 2.9 $(1 - X_r)^{2/3}$ for $X_r = 0.3$ corresponding to propane. This C_T is related to the previous far-field values of the infinite line and (point) axisymmetric sources, but we have not tried to unify these results further. The preceding solution does converge to the correct limiting geometric behavior.

In the combusting region, we simply fit the rectangular data as $\Phi = 0.421\Psi$, which corresponds to the limiting values of 0.35Ψ and 0.45Ψ of Table 3.

W can be computed from the application of condition 2 with the selection of the constant C as 1.5. The entrainment equation can be written as

$$\dot{m}_e = 4\int_0^x \int_0^\infty \rho_\infty w\, dx\, dy = \pi\rho_\infty w_m ab \qquad (14)$$

Accordingly, the entrainment expressions can be determined for each plume region. By equations 9 or 12, where Φ is constant, the flame height can be determined from the expression

$$Q^*_{mod} = C_f\left(\frac{Z_f}{D}\right)^{1/2}\left[1 + 2C_1\left(\frac{Z_f}{D}\right)\right] \times \left[1 + 2C_1\left(\frac{D}{L}\right)\left(\frac{Z_f}{D}\right)\right]$$

$$\text{with } C_f = 0.00590\left(\frac{\Psi^{3/2}}{1 - X_r}\right) \text{ and } C_1 = 0.199 \qquad (15)$$

We have retained the same C_f used in both the axisymmetric and line cases as given in Table 5. The C_1 value for the rectangular data fit is slightly higher than the axisymmetric flame region result. At some point, for D/L small enough (roughly <0.1), C_1 must increase to the larger infinite line value of Table 5. A refinement might include an inclusion of a D/L effect on C_1 for the rectangular case.

Conclusions

We have formulated a unified analysis that correctly expresses the behavior of finite axisymmetric and rectangular fire plumes. An incorporation of flame radiation loss, X_r, shows that this parameter is

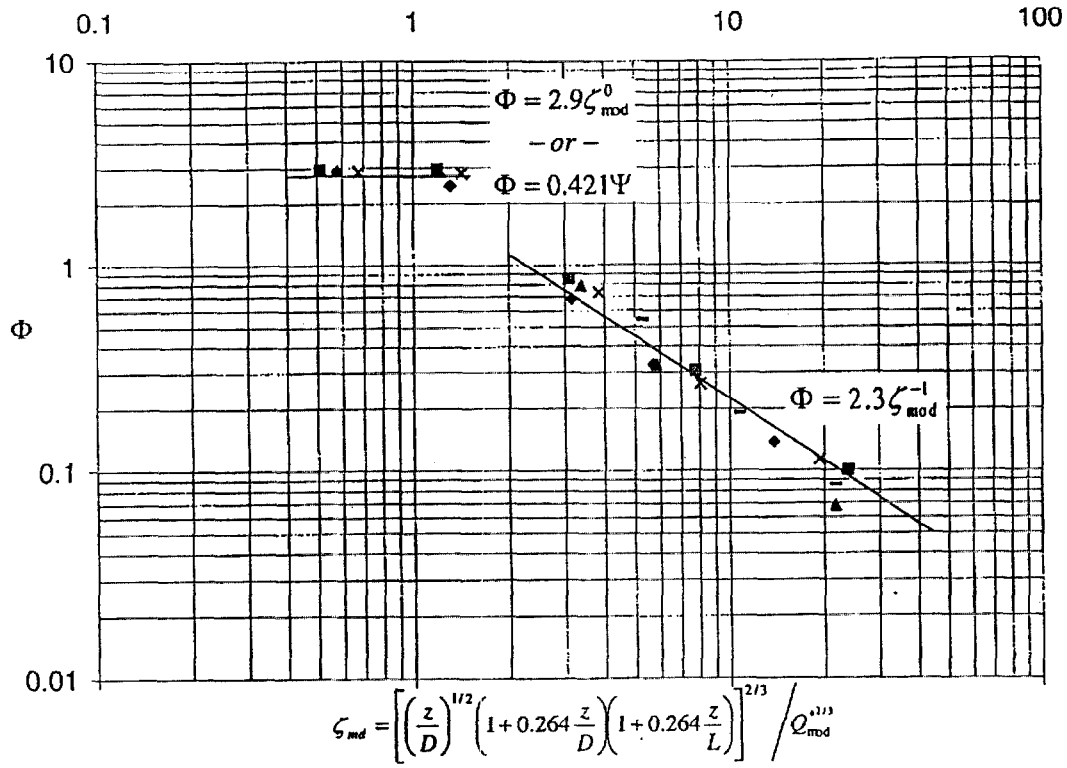

FIG. 6. Dimensionless temperature versus height for rectangular sources. ♦ Hasemi and Nishita (0.2 × 1.0 m) [12]; ■ Hasemi (0.2 × 0.8 m); ▲ Hasemi (0.2 × 0.6 m); × Hasemi (0.2 × 0.4 m); ▬ Hasemi (0.2 × 0.2 m).

a significant factor that permeates the analysis, and, consequently, it is recommended that future experimental studies report X_r. Low Q^* values show distinctive dependence on D and fire source geometric effects that suggest the influence of Gr number effects in addition to the D dependence given by the theory presented herein.

Nomenclature

a half-length variable
b half-width or radius of plume
B dimensionless length variable, equation 2
c_p specific heat (1.01 kJ/kg-K)
C_i generic constants used in equations
D diameter or line width
g gravity (9.81 m/s^2)
L length of rectangular fuel source
m mass
n fraction of stoichiometric air entrained
Q energy release
r radius in polar coordinates
s stoichiometric air-to-fuel mass ratio
T Temperature (T_o = 293 K)
v horizontal velocity
w vertical velocity
W dimensionless velocity (equation 2)
x horizontal coordinate parallel to length
X_r radiation loss fraction
y horizontal coordinate parallel to width
z vertical coordinate
Z_c characteristic plume length scale (equation 3)

Greek Symbols

α dimensionless entrainment coefficient
β Gaussian profile constant
$\Delta H_c/s$ heat of combustion per unit mass of air (2.91 kJ/g)
ρ density (ρ_o = 1.21 kg/m^3
Φ dimensionless temperature, equation 2
ζ dimensionless height ratio, equation 2
Ψ dimensionless parameter, equation 5

Subscripts

e entrained air
f flame
m maximum or centerline value
o ambient conditions

Superscripts

() signifies rate of change
( )′ single prime (per unit length)
( )″ double prime (per unit area)
( )‴ triple prime (per unit volume)

Acknowledgments

We are grateful to the support for this study from National Institute of Standards and Technology/Building and Fire Research Laboratory and Dr. David Evans.

REFERENCES

1. Yokoi, S., *Study on the Prevention of Fire Spread Caused by Hot Upward Current*, Building research report 34, Japanese Ministry of Construction, 1960.
2. Rouse, H., Yih, C. S., and Humphries, H. W., *Tellus* 4:202–210 (1952).
3. Morton, B. R., Taylor, G. I., and Turner, J. S., *Proc. of the Royal Soc. of London, Ser. A* 234:1–23 (1956).
4. McCaffrey, B. J., *Purely Buoyant Diffusion Flames: Some Experimental Results*, National Bureau of Standards report NSBIR 79-1910.
5. Cox, G. and Chitty, R., *Combust. Flame* 39:191–209 (1980).
6. Zukoski, E. E., in *First Symposium (International) on Fire Safety Science*, 1985, pp. 1–11.
7. Heskestad, G., *Combust. Flame* 83:293–301 (1991).
8. Lee, S. L. and Emmons, H. W., *J. of Fluid Mech.* 11:353–368 (1961).
9. Thomas P. H., in *Ninth Symposium (International) on Combustion*, Academic Press, New York, 1963, pp. 844–859.
10. Steward, F. R., *Combust. Flame* 8:171–178 (1964).
11. Steward, F. R., *Combust. Sci. Technol.* 2:203–212 (1970).
12. Hasemi, Y. and Nishita, M., in *Second Symposium (International) on Fire Safety Science*, Hemisphere, New York, 1988, pp. 275–284.
13. Sugawa, O., Yasushi, O., and Satoh, H., in *Third Symposium (International) on Fire Safety Science*, 1991, pp. 435–444.
14. Yuan, L. and Cox, G., *Fire Safety J.* 27:123–139 (1996).
15. Sugawa, O., Yasushi, O., and Hirofumi, H., *Fire Induced Flow in a Clean Room with Downward Vertical Laminar Flow*, National Bureau of Standards report NSBIR 88-3753, 1987.
16. Thomas, P. H., Webster, C. T., and Raftery, M. M., *Combust. Flame* 5:359–367 (1961).
17. Delichatsios, M. A., *Combust. Flame* 70:33–46 (1987).
18. Roper, F. G., *Combust. Flame* 91:226–238 (1992).
19. Roper, F. G., Smith, C., and Cunningham, A. C., *Combust. Flame* 29:227–234 (1977).
20. Grove, B. S., "Correlations for Infinite Line Fires," MS thesis, Department of Fire Protection Engineering, University of Maryland, College Park, MD, Dec. 1997.
21. Zukoski, E. E., "Properties of Fire Plumes," *Combustion Fundamentals of Fire*, (G. Cox, ed.), Academic Press, London, 1995, p. 121.
22. Brodowicz, K. and Kierkus, K. T., *Int. J. Heat Mass Transfer* 9:81–94 (1966).
23. Cox, G. and Chitty, R., *Combust. Flame* 60:219–232 (1985).
24. Baum, H. R. and McCaffrey, B. J., in *Second Symposium (International) on Fire Safety Science*, 1988, pp. 129–148.
25. Zukoski, E. E., in *Fourth Symposium (International) on Fire Safety Science*, 1994, pp. 137–147.
26. Smith, R. K. and Morton, B. R., *J. of Fluid Mech.* 68/1:1–19 (1975).
27. McCaffrey, B., "Flame Heights," *SFPE Handbook of Fire Protection Engineering*, 2nd ed., National Fire Protection Association, Quincy, MA, 1995.
28. Taminini F., *Combust. Flame* 30:85–101 (1977).
29. Hamins A., Konishi, K., Borthwick, P., and Kashiwagi, T., in *Twenty-Sixth Symposium (International) on Combustion*, The Combustion Institute, Pittsburgh, 1996, pp. 1429–1436.
30. Ricou, F. P. and Spalding, B. P., *J. Fluid Mech.* 11:21–32 (1961).

COMMENTS

Bruce Gerhold, Phillips Petroleum, USA. Even though ground-level wind may be near zero, the atmosphere is almost never calm for altitudes of interest (0–1000 m) for plume rise. Can you suggest any crosswind correction procedure?

Author's Reply. This issue of a crosswind will include another dimensionless group in the solution, namely, $V_{wind}/(gZ^*)^{1/2}$, as well as possibly D/Z^*. Many empirical correlations can be found in the literature, but their uncertainty is greater than for the ambient plume. As far as plume rise in the atmosphere to heights of 1000 m and above, there are two issues of concern. The density variation of the atmosphere with height is a factor. This variation can cause either stratification for an atmosphere that has a density inversion (decreasing) or an increase in buoyancy due to a normal atmosphere (decreasing temperature) from condensation that can occur within the plume from moisture in the ambient air. Both effects have been addressed.